




# The enhanced multiferroic properties of BiFeO<sub>3</sub> composite film by doping ions in the magnetic layer

Jincheng Li<sup>1,\*</sup> , Guoqiang Tan<sup>1</sup>, Xixi Ren<sup>1</sup>, Di Ao<sup>1</sup>, Chenjun Liu<sup>1</sup>, Huijun Ren<sup>2</sup>, Ao Xia<sup>1</sup>, and Wenlong Liu<sup>3</sup>

<sup>1</sup> Shaanxi Key Laboratory of Green Preparation and Functionalization for Inorganic Materials, School of Materials Science and Engineering, Shaanxi University of Science & Technology, Xi'an 710021, Shaanxi, China

<sup>2</sup> School of Arts and Sciences, Shaanxi University of Science & Technology, Xi'an 710021, Shaanxi, China

<sup>3</sup> School of Electronic Information and Artificial Intelligence, Shaanxi University of Science & Technology, Xi'an 710021, Shaanxi, China

Received: 28 October 2020

Accepted: 26 December 2020

Published online:

23 January 2021

© The Author(s), under exclusive licence to Springer Science+Business Media, LLC part of Springer Nature 2021

## ABSTRACT

Bi<sub>0.88</sub>Gd<sub>0.09</sub>Sr<sub>0.03</sub>Fe<sub>0.94</sub>Mn<sub>0.04</sub>Co<sub>0.02</sub>O<sub>3</sub>/Co<sub>1-x</sub>Ni<sub>x</sub>Fe<sub>2</sub>O<sub>4</sub> (BGSFMC/CN<sub>x</sub>FO,  $x = 0.1-0.5$ ) composite films were successfully prepared by the sol-gel method. The structure and performance changes of BGSFMC/CN<sub>x</sub>FO composite film were studied. The results show that after the Ni<sup>2+</sup>-doped CN<sub>x</sub>FO magnetic bottom layer is combined with the upper BGSFMC, stress is generated in the film interface, which makes the upper BGSFMC layer phase structure change from a single R3c:H phase to the coexistence of R3c:H and R3m:R phases. The change of the structure causes the Fe–O bond length and Fe–O–Fe bond angle of the upper layer of the BGSFMC to change, the internal oxygen vacancy concentration decreases and the Fe<sup>3+</sup> concentration increases. As a result, the inclination of the upper BGSFMC layer octahedron changes, limiting spatial modulation and releasing magnetism. At the same time, the change of structure also inhibits the conversion of Fe<sup>3+</sup> to Fe<sup>2+</sup> and strengthens the spin tilt and Fe–O–Fe super exchange interaction to enhance ferromagnetism. The ferromagnetic properties of the BGSFMC/CN<sub>x</sub>FO composite film are significantly enhanced, and the residual magnetization of 48.29–56.94 emu/cm<sup>3</sup> is obtained. The reduction of defect complexes makes the ferroelectric domains of the BGSFMC/CN<sub>x</sub>FO composite film easier to flip under an external electric field, the symmetry and peak sharpness of the C–V characteristic curve increase, and the intrinsic polarization increases. The BGSFMC/CN<sub>0.1</sub>FO composite film obtained an increased Pr = 112 μC/cm<sup>2</sup>, a polarization switching current I<sub>s</sub> = 0.081 mA, a ferroelectric domain switching capacitance peak C<sub>S</sub> = 24.9 μF/cm<sup>2</sup>, and a reduced leakage conductivity C<sub>L</sub> = 4.73 μF/cm<sup>2</sup>. Through the ion doping of the magnetic layer, the ferromagnetic and ferroelectric properties of the BFO film can be adjusted and improved.

Address correspondence to E-mail: lijincheng0104@163.com

## 1 Introduction

With the development of technologies such as artificial intelligence, cloud computing, 5G, and big data, the semiconductor industry is facing severe challenges. Materials with a single function can no longer meet the needs of development. The high integration, multi-function, and miniaturization of equipment are the future trends. Multiferroic materials have a wide range of application prospects in the field of multifunctional materials because of the coupling between various ferrous properties. On this basis, BiFeO<sub>3</sub> has a high ferroelectric phase transition temperature and spontaneous polarization strength as high as 100 μC/cm<sup>2</sup>, becoming a representative of multiferroic materials and has attracted widespread attention. The study has found that the ferroelectricity of BiFeO<sub>3</sub> comes from Bi ions compared with the deviation of the center of FeO<sub>6</sub> octahedron. This deviation is mainly caused by the hybridization of the lone pair of electrons existing on the 6s orbital of Bi ions with the surrounding oxygen atoms [1–6]. In the BFO structure, the magnetic moment of Fe<sup>3+</sup> is in a ferromagnetic order in the [111] plane, while the magnetic moments of two adjacent Fe<sup>3+</sup> in the [111] direction are arranged in anti-parallel to form an anti-ferromagnetic structure [7]. The spin of the adjacent FeO<sub>6</sub> octahedron along the [111] polarization axis causes the tilt of the Fe<sup>3+</sup> magnetic moment, while the magnetic moment in the opposite direction cannot be completely offset, resulting in the formation of weak magnetism. In order to push BiFeO<sub>3</sub> into practical applications, researchers have made many efforts to improve ferroelectric and ferromagnetic properties [8, 9]. However, the degree of improvement in its ferroelectric and ferromagnetic properties is relatively low. Further research found that doping transition metals at the Fe site could effectively enhance the ferromagnetism of BFO [10], causing more people to focus on the multiple co-doping of A and B sites. Liu et al. [11] successfully prepared BLEFMC films in which La and Er were doped at the Bi site while Mn and Co were doped at the Fe site. The multi-element ion doping reduced the built-in electric field formed by the defects or the defect pairs in the film and decreased the grain size, grain boundary resistance, oxygen vacancy, and the Fe<sup>2+</sup> content. A high remanent polarization of 152 μC/cm<sup>2</sup> was obtained. However, its ferromagnetic properties

( $M_s = 2.32 \text{ emu/cm}^3$ ) were still very weak. Chai et al. [12] doped Gd and Sr at the A site, and Mn and Co at the B site of the BFO film. The formation of oxygen vacancies in the BSG<sub>x</sub>FMC film was inhibited by the multi-element doping, which led to the decrease in the built-in electric field of the depletion layer formed between the gold electrode and the BFO ferroelectric layer. The offset phenomenon of the coercive field was weakened, which revealed the good ferroelectric properties (134 μC/cm<sup>2</sup>). However, the ferromagnetic properties had not been improved ( $M_s = 2.64 \text{ emu/g}$ ). To address this drawback, the combination of magnetic spinel (NiFe<sub>2</sub>O<sub>4</sub>, MnFe<sub>2</sub>O<sub>4</sub>, CoFe<sub>2</sub>O<sub>4</sub>, etc.) and BiFeO<sub>3</sub> to form a composite film [13–15], the coexistence of ferroelectric and ferromagnetic phases to improve the weak ferromagnetic properties of BFO is an effective choice. Guo et al. [16] prepared BSrSFMC/NFO composite films by doping Sr and Sm at the Bi site while doping Mn and Co at the Fe site, which was then combined with NiFe<sub>2</sub>O<sub>4</sub>. It has obtained considerable ferroelectric properties (Pr = 88.28 μC/cm<sup>2</sup>). However, the ferromagnetic properties ( $M_s = 35.7 \text{ emu/cm}^3$ ) were significantly lower than those of NiFe<sub>2</sub>O<sub>4</sub> films. Tan et al. [17] prepared Bi<sub>0.9</sub>Er<sub>0.1</sub>Fe<sub>0.96</sub>Mn<sub>0.02</sub>Co<sub>0.02</sub>O<sub>3</sub>/Co<sub>1-x</sub>Mn<sub>x</sub>Fe<sub>2</sub>O<sub>4</sub> (BEFMC/CM<sub>x</sub>FO) composite film. The doping of Mn ions in the bottom layer caused the structural transformation of the BFO layer to form a weak local electric field, which led to a weak interface effect. Then, the enhanced ferroelectric properties (Pr ~ 157.8 μC/cm<sup>2</sup>) and ferromagnetic properties ( $M_s \sim 51.47 \text{ emu/cm}^3$ ) were obtained. However, the ferromagnetic performance of the BEFMC/CM<sub>x</sub>FO composite film was generally lower than that of the BEFMC/CFO composite film. Chai et al. [18] prepared Bi<sub>0.88</sub>Sr<sub>0.03</sub>Gd<sub>0.09</sub>Fe<sub>0.94</sub>Mn<sub>0.04</sub>Co<sub>0.02</sub>O<sub>3</sub>/Co<sub>1-y</sub>Mn<sub>y</sub>Fe<sub>2</sub>O<sub>4</sub> (BSGFMC/CM<sub>y</sub>FO) composite film. The structural distortion caused by the doping of Mn<sup>2+</sup> ions in the CM<sub>y</sub>FO film of the magnetic layer induced the transition of the upper BSGFMC film in the composite film from the trigonal structure of the R3c:H and R3m:R space groups to the single R3m:R space group. The enhanced ferroelectric properties (Pr ~ 106 μC/cm<sup>2</sup>) were obtained and the coercive field (263 kV/cm) was reduced. However, the magnetic properties of the BSGFMC/CM<sub>y</sub>FO composite film were still worse than those of the BSGFMC/CFO composite film.

Based on the previous researchers, the upper layer of the composite film is multi-doped with BFO and

the lower layer is doped with transition metal elements to form a weak local electric field and the weak interface effects, resulting in the enhanced ferroelectric properties. However, the ferromagnetic properties of the composite film are lower than those of the composite film without the magnetic layer doped with transition metal elements. How to improve the ferroelectric performance of the composite film but to enhance the ferromagnetic performance of the composite film is still a problem that needs to be solved in the practical application of BFO. Compared with other technologies, the sol–gel method has the advantages of low cost, simple synthesis equipment, and molecular-level doping [19–21]. In this work, the sol–gel method was selected to prepare  $\text{Bi}_{0.88}\text{Gd}_{0.09}\text{Sr}_{0.03}\text{Fe}_{0.94}\text{Mn}_{0.04}\text{Co}_{0.02}\text{O}_3/\text{Co}_{1-x}\text{Ni}_x\text{Fe}_2\text{O}_4$  (BGSFMC/ $\text{CN}_x\text{FO}$ ) composite film by doping  $\text{Ni}^{2+}$  ions into the CFO magnetic layer. Through the formation of internal stress at the film interface, the structure of the upper BGSFMC is induced to enhance the ferromagnetic properties of the composite film while enhancing the ferroelectric properties.

## 2 Experimental

$\text{Bi}_{0.88}\text{Gd}_{0.09}\text{Sr}_{0.03}\text{Fe}_{0.94}\text{Mn}_{0.04}\text{Co}_{0.02}\text{O}_3/\text{Co}_{1-x}\text{Ni}_x\text{Fe}_2\text{O}_4$  (BGSFMC/ $\text{CN}_x\text{FO}$ ,  $x = 0.0, 0.1, 0.3, 0.5$ ) composite films were fabricated on the FTO/glass substrates by using the sol–gel method. To prepare the BGSFMC precursor solutions, the raw materials of  $\text{Bi}(\text{NO}_3)_3 \cdot 5\text{H}_2\text{O}$  (5% excess),  $\text{Gd}(\text{NO}_3)_3 \cdot 6\text{H}_2\text{O}$ ,  $\text{Sr}(\text{NO}_3)_2$ ,  $\text{Fe}(\text{NO}_3)_3 \cdot 9\text{H}_2\text{O}$ ,  $\text{C}_4\text{H}_6\text{MnO}_4 \cdot 4\text{H}_2\text{O}$ , and  $(\text{Co}(\text{NO}_3)_2 \cdot 6\text{H}_2\text{O})$  were dissolved into ethylene glycol methyl ether and acetic anhydride (the volume ratio was 3:1). The as-prepared precursor solutions were stirred for 2 h and aged for 24 h at room temperature to form the homogeneous precursor solutions (0.3 mol/L). For the preparation of  $\text{CN}_x\text{FO}$  precursor solutions,  $\text{Co}(\text{NO}_3)_2 \cdot 6\text{H}_2\text{O}$ ,  $\text{C}_4\text{H}_6\text{NiO}_4 \cdot 4\text{H}_2\text{O}$ , and  $\text{Fe}(\text{NO}_3)_3 \cdot 9\text{H}_2\text{O}$  were dissolved in ethylene glycol methyl ether and acetic anhydride (the volume ratio was 3:1). The as-fabricated precursor solutions were stirred for 2 h and aged for 24 h at room temperature to obtain the homogeneous precursor solutions with the 0.2 mol/L concentration. The BGSFMC/ $\text{CN}_x\text{FO}$  composite films were fabricated by spin coating the two precursor solutions onto the FTO/glass substrates. The  $\text{CN}_x\text{FO}$  layers were first deposited on the FTO/glass substrates by spin coating at 4000 r/min for 15 s and the

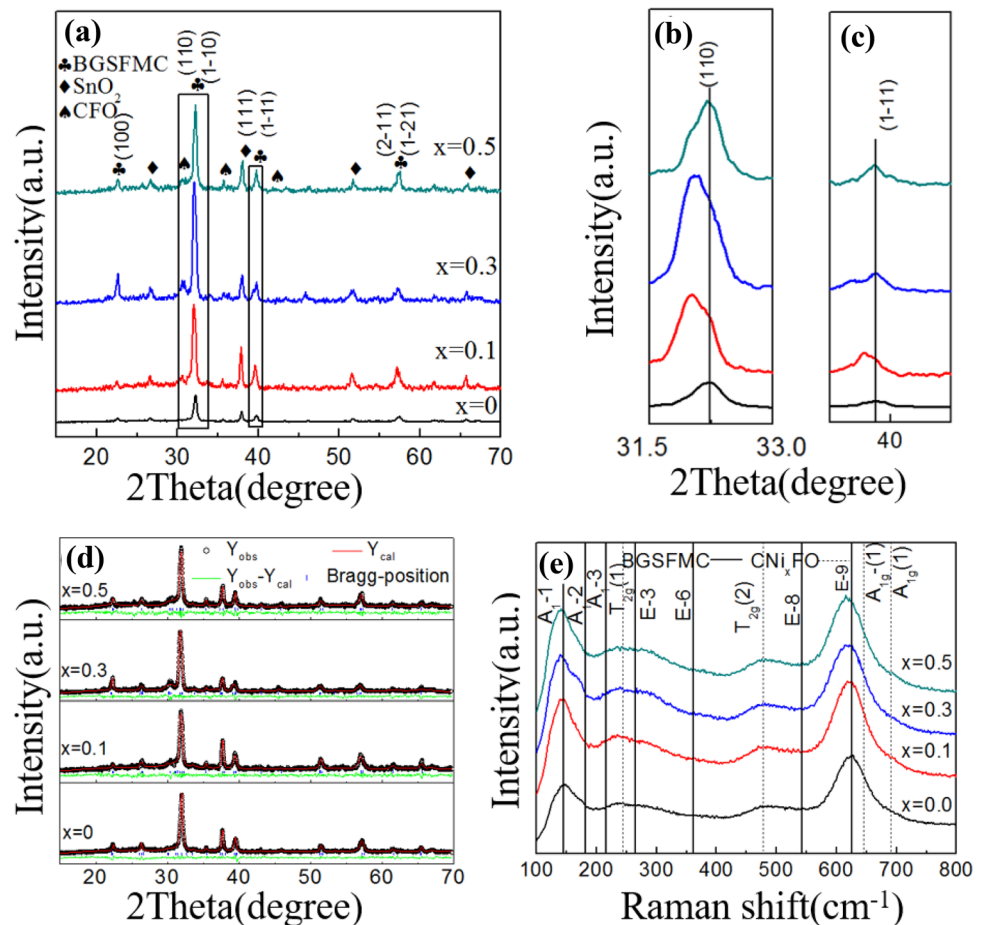
wet films were dried at 200 °C for 8 min. Then, the as-prepared dried films were annealed at 600 °C for 20 min to allow crystallization. The above procedures were repeated six times for the  $\text{CN}_x\text{FO}$  layer. Finally, BGSFMC layers were deposited on the  $\text{CN}_x\text{FO}/\text{FTO}/\text{glass}$  by spin coating at 4000 r/min for 15 s and the wet films were dried at 200 °C for 8 min. The as-prepared dried films were annealed at 550 °C for 10 min to obtain the crystallized films. The above process was repeated 13 times for fabricate the BGSFMC layer. To test the electric behaviors, an Au top electrode with  $0.03 \text{ mm}^2$  was sputtered on the surface of the thin films and then annealed at 285 °C for 20 min.

An X-ray diffractometer (XRD, D/MAX-2200, Rigaku Cu) was used to characterize the structure and crystallinity of the film under the conditions of Cu target  $K\alpha$  rays, X-ray wavelength of 0.15418 nm, tube current of 40 mA, and tube voltage of 40 kV. A Horiba JYHR800 Raman system equipped with 532 nm Ar ion laser excitation was used to study the Raman spectra. A field emission scanning electron microscope (FESEM, S4800, Hitachi) was used to observe the surface morphology and the interface contact of the film. An X-ray photoelectron spectroscopy (XPS) of Kratos XSAM800 spectrometer was used to analyze the surface element composition and the ion valence of the sample. An Aix ACCT TF-Analyzer 2000 was used to test the hysteresis loop. The magnetic properties were determined by a superconducting quantum interference magnetic measuring system (SQUID MPMSXL-7).

## 3 Results and discussions

Figure 1a is the XRD pattern of the BGSFMC/ $\text{CN}_x\text{FO}$  composite film. The BGSFMC layer of the composite film conforms to the PDF standard card (JCPDS No. 20-0169), which is a polycrystalline twisted perovskite trigonal structure, and the space group is R3c. The  $\text{CN}_x\text{FO}$  layer conforms to the PDF standard card (JCPDS No. 22-1088), which is a cubic structure and the space group is Fd-3m. It indicates that there is no formation of intermediate compounds in the composite film and also indicates that the BFO phase and the CFO phase coexist. With the lower layer of  $\text{Ni}^{2+}$ -doped CFO, the (1–10) crystal plane diffraction peak and (1–11) crystal plane diffraction peak of the upper layer of BGSFMC are shifted to a small angle. The

**Fig. 1** The structure of BGSFMC/CN<sub>x</sub>FO composite film **a** XRD; **b** 31.5°–33° XRD; **c** 39°–41° XRD; **d** refined graph; **e** Raman spectrum



diffraction peak intensity is significantly enhanced. From the observation of the BGSFMC/CN<sub>x</sub>FO composite film, there are obvious upper BGSFMC (1–10) crystal plane diffraction peaks, and (1–11) crystal plane diffraction peaks are reverted to higher angles (Fig. 1b and c). This is because the doping of Ni<sup>2+</sup> causes the structure of the CN<sub>x</sub>FO layer to change, and the formation of stress at the interface of the film causes the structure of the upper BGSFMC to change. In S1, the structural changes of the CN<sub>x</sub>FO films are further explained. Maud software is used to perform Rietveld-refined fitting of XRD data (Fig. 2d and Table 1). The structure of the upper BGSFMC of the BGSFMC/CFO composite film is 98.92% tripartite R3c:H and 1.08% tripartite R3m:R, which is almost a single-phase tripartite R3c:H structure. When the doping amount of Ni<sup>2+</sup> is 0.1, the structure of the upper BGSFMC is a two-phase coexistence of tripartite R3c:H (52.44%) and tripartite R3m:R (47.56%). When the doping amount is 0.5, the structure of the upper BGSFMC is almost the single-phase tripartite

R3c:H (92.39%). The amount of Ni<sup>2+</sup> doping in the lower CFO is increased, the structure of BGSFMC/CN<sub>x</sub>FO is changed from a single-phase tripartite R3c:H to a tripartite R3c:H and tripartite R3m:R where two phases coexist. Then from the tripartite R3c:H and the tripartite R3m:R, the two phases coexist to the tripartite R3c:H single phase. The Ni<sup>2+</sup>-doped lower CFO layer can affect the growth orientation of the upper BGSFMC crystal. The Ni<sup>2+</sup>-doped lower CFO can cause the structural distortion of the crystal and change the Fe–O bond length and the Fe–O–Fe bond angle of the upper BGSFMC layer. Figure 1e is the Raman scattering spectrum of the BGSFMC/CN<sub>x</sub>FO composite film. The vibration peaks at 148 and 604 cm<sup>-1</sup> correspond to the vibration modes of A<sub>1</sub>-1 and E-9 in the upper BGSFMC of the composite film [22]. The vibration peaks of 237 and 471 cm<sup>-1</sup> correspond to the vibration modes of T<sub>2g</sub>(1) and T<sub>2g</sub>(2), respectively, of the CN<sub>x</sub>FO under the composite film [23]. The low-frequency A mode and the high-frequency E mode of BGSFMC are

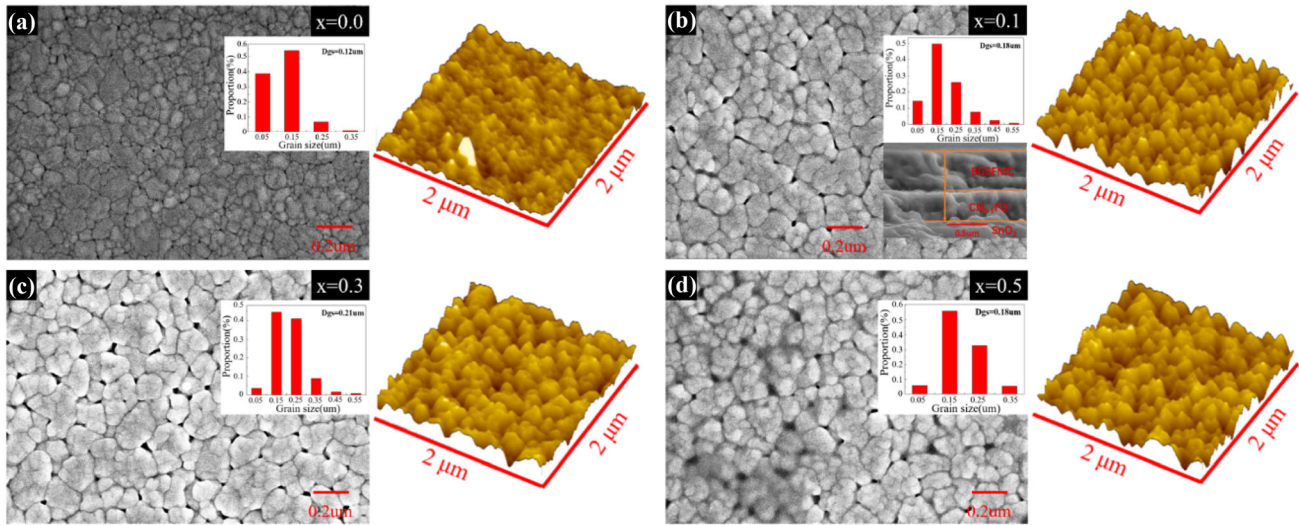


**Fig. 2** The SEM of the BGSFMC/CN<sub>x</sub>FO composite film and the corresponding AFM. The inset is the grain size distribution and the cross-sectional SEM

**Table 1** Structural parameters of the BGSFMC/CN<sub>x</sub>FO composite film

Samples	Crystal structure	Space group	Lattice parameters		Fe–O bond length	Fe–O–Fe bond angle
			<i>a</i>	<i>c</i>		
BGSFMC/CFO	Trigonal	R3c:H (98.92%)	5.60	14.06	1.757	79.57
		R3m:R (1.08%)	3.95		1.98	0
BGSFMC/CN <sub>0.1</sub> FO	Trigonal	R3c:H (52.44%)	5.72	14.35	1.452	114.299
		R3m:R (47.56%)	3.96		1.816	0
BGSFMC/CN <sub>0.3</sub> FO	Trigonal	R3c:H (25.68%)	5.64	14.72	1.901	59.676
		R3m:R (74.32%)	3.97		1.98	0
BGSFMC/CN <sub>0.5</sub> FO	Trigonal	R3c:H (92.39%)	5.58	14.25	1.712	48.003
		R3m:R (7.61%)	3.96		1.98	0

related to the vibration of Bi–O and Fe–O bonds [24]. The doping of Ni<sup>2+</sup> in the lower CFO can increase the vibration mode strength of A<sub>1</sub>-1 and E-9 of the upper BGSFMC of the composite film, which proves that the doping of Ni<sup>2+</sup> in the lower CFO induces changes in the structure of the upper BGSFMC, which is consistent with the changes in XRD. These phenomena indicate that the structure change of the lower layer CN<sub>x</sub>FO can be controlled by doping Ni<sup>2+</sup> to control the transformation of the upper-layer BGSFMC structure.

Figure 2 shows the SEM of the BGSFMC/CN<sub>x</sub>FO composite film and the corresponding AFM. Obviously, the BGSFMC/CN<sub>x</sub>FO composite film shows a relatively dense and uniform morphology. The average grain size (*D<sub>gs</sub>*) of the BGSFMC/CN<sub>x</sub>FO

composite film is 0.12, 0.18, 0.21, and 0.18 μm, respectively. The inset of Fig. 2b is a cross-sectional view of the BGSFMC/CN<sub>0.1</sub>FO composite film. The three-layer structure can be clearly observed: the upper BGSFMC layer, the lower CN<sub>x</sub>FO layer, and the SnO<sub>2</sub> substrate. The interface between the three layers is clear. The thickness of the BGSFMC/CN<sub>0.1</sub>FO composite film is 705 nm. The AFM test range is 2 μm × 2 μm. With the doping of Ni<sup>2+</sup>, the average particle size of the BGSFMC/CN<sub>x</sub>FO composite film is about 100 nm, 150 nm, 200 nm, and 160 nm, which are consistent with the SEM analysis. The increase in the average particle size means that the ferroelectric domain size of the film increases. The increase of peak-like protrusions on the surface of the film indicates that the surface roughness of the film

has increased and the pores have increased. The change of surface morphology and grain size with  $\text{Ni}^{2+}$  doping is related to the influence of internal stress on grain evolution. The doping of  $\text{Ni}^{2+}$  causes internal stress to cause the grain growth of the upper layer of the film, and the structure of the film is distorted, providing space for changes in the Fe–O–Fe bond angle and Fe–O bond length.

Figure 3 shows the XPS spectrum of the BGSFMC/ $\text{CN}_x\text{FO}$  composite film. From Fig. 3a, it can clearly be found that there are the characteristic peaks of Bi, Gd, Sr, Fe, Mn, Co, and O elements. Figure 3b shows the spectrum of Fe-2p orbitals. Fitting by Avantage software confirms that Fe-2p<sub>3/2</sub> characteristic peak is split into two peaks:  $\text{Fe}^{3+}$  and  $\text{Fe}^{2+}$ . The ratio of  $\text{Fe}^{3+}$  and  $\text{Fe}^{2+}$  content in the BGSFMC/ $\text{CN}_x\text{FO}$  ( $x = 0.0$ – $0.5$ ) composite film is calculated to be 11:89, 15:85, 18:82, and 20:80, respectively. Figures 3c and d are the characteristic peak patterns of Co-2p and Mn-2p. There are both  $\text{Co}^{3+}/\text{Co}^{2+}$  and  $\text{Mn}^{3+}/\text{Mn}^{2+}$  in the composite film. The ratios of  $\text{Co}^{3+}$  and  $\text{Co}^{2+}$  in the BGSFMC/ $\text{CN}_x\text{FO}$  ( $x = 0.0$ – $0.5$ ) composite film are 81:19, 81:19, 86:14, and 87:13, respectively. The ratios of  $\text{Mn}^{3+}/\text{Mn}^{2+}$  are 20:80, 29:71, 25:75, and 20:80, respectively. The existence of  $\text{Mn}^{3+}/\text{Mn}^{2+}$  and  $\text{Co}^{3+}/$

$\text{Co}^{2+}$  can maintain the charge balance in the film. It can also inhibit the conversion from  $\text{Fe}^{3+}$  to  $\text{Fe}^{2+}$  and the formation of oxygen vacancies. This mechanism can be expressed by the following defect reaction Eqs. (1), (2), (3), and (4) [25]:

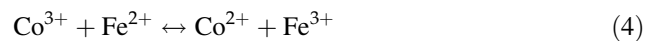
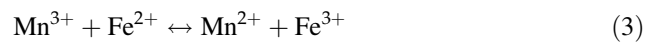
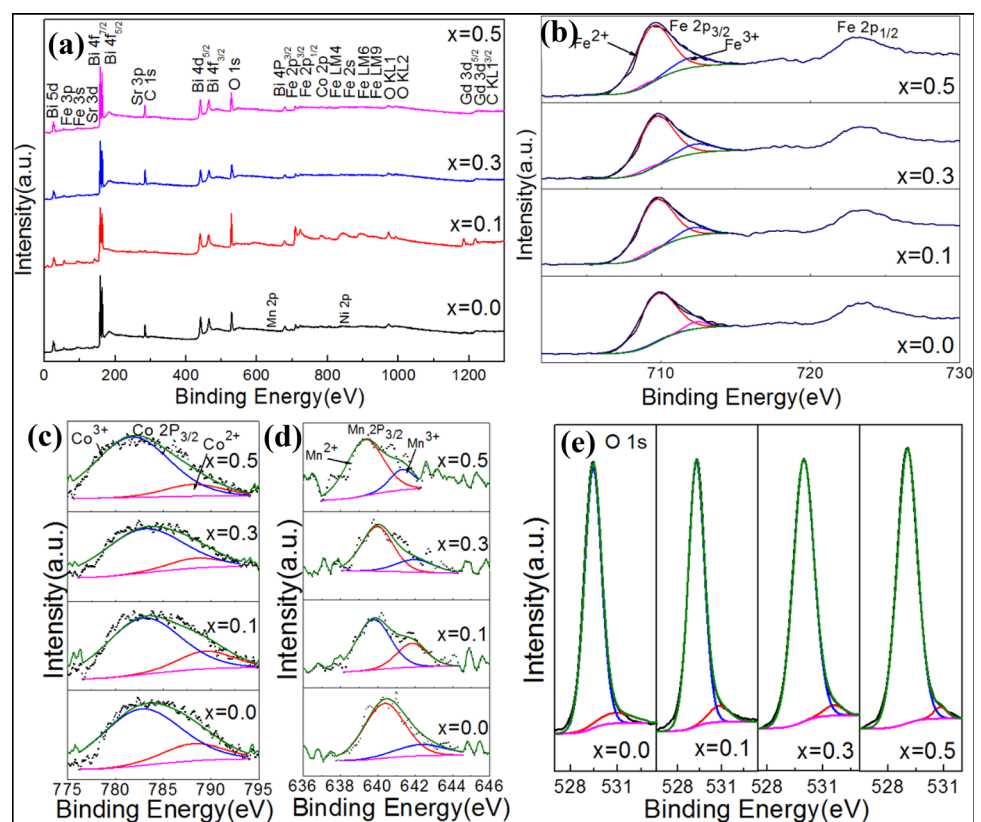


Figure 3e shows the O1s characteristic peak spectrum of the BGSFMC/ $\text{CN}_x\text{FO}$  composite film XPS. The ratios of  $\text{O}^{2-}$  and oxygen vacancies in the BGSFMC/ $\text{CN}_x\text{FO}$  composite film ( $x = 0.0$ – $0.5$ ) are 92.18:7.82, 92.75:7.25, 96.47:3.53, and 97.23:2.67, respectively, indicating that the oxygen vacancy of the composite film is significantly reduced. Through the  $\text{Ni}^{2+}$ -doped  $\text{CN}_x\text{FO}$  film, the Ni–O bond is formed in the lower layer, which changes the translational movement of octahedral  $\text{FeO}_4$  and forms the internal stress in the film interface. It promotes the growth of the upper BGSFMC crystal grains, inhibits

**Fig. 3** a XPS full spectra of the BGSFMC/ $\text{CN}_x\text{FO}$  composite film ( $x = 0.0$ – $0.5$ ), b Fe-2p, c Co-2p, d Mn-2p, and e O1s spectra



the conversion from Fe<sup>3+</sup> to Fe<sup>2+</sup> in the upper BGSFMC crystal, and reduces oxygen vacancies.

Figure 4 shows the hysteresis loop of CN<sub>x</sub>FO film and BGSFMC/CN<sub>x</sub>FO composite film at room temperature. The ferromagnetic properties of the composite film are mainly derived from the underlying magnetic material. As shown in Fig. 4a, the residual magnetization is 124.43 emu/cm<sup>3</sup>, 126.30 emu/cm<sup>3</sup>, 105.88 emu/cm<sup>3</sup>, and 122.72 emu/cm<sup>3</sup>, respectively. With the incorporation of Ni<sup>2+</sup>, the magnetic properties of the underlying CN<sub>x</sub>FO film are significantly reduced (Fig. 4a). However, the magnetic properties of the BGSFMC/CN<sub>x</sub>FO composite film show a significant enhancement, as shown in Fig. 4b, the residual magnetization is 29.74 emu/cm<sup>3</sup>, 56.94 emu/cm<sup>3</sup>, 51.56 emu/cm<sup>3</sup>, and 48.29 emu/cm<sup>3</sup>. The results show that adjusting the structure of the lower magnetic layer can enhance the ferromagnetic properties of the BGSFMC/CN<sub>x</sub>FO composite film. After the Ni<sup>2+</sup>-doped CN<sub>x</sub>FO magnetic bottom layer is combined with the upper BGSFMC, the film interface generates stress, which makes the film phase structure change from a single R3c:H phase to the coexistence of R3c:H and R3m:R phases. This results in an increase in the grain size and porosity of the upper BGSFMC layer, which provides a space for changes in the Fe–O bond length and Fe–O–Fe bond angle of the BGSFMC layer. The changes of the Fe–O bond length and the Fe–O–Fe bond angle cause the spin tilt [26], resulting in the change of the octahedral tilt, which further limits the spatial modulation and releases the magnetism [27]. The tilt of Fe<sup>3+</sup> ion spin is related to the Dzyaloshinskii–Moriya (DM) interaction energy of Fe<sup>3+</sup> ion (HDM):

$$H_{DM} = \sum_{n=0}^n \vec{D}_n \cdot \left( \vec{s}_0 \times \vec{s}_n \right), \tag{5}$$

where  $D_n = V_0 \left[ \vec{r}_{n-0} \times \vec{r}_{n-n} \right]$  is the interaction parameter of DM interaction,  $\vec{r}_{n-0}$  and  $\vec{r}_{n-n}$  are the position vectors of the closest magnetic ion from the  $n$ th O ion to the closest Fe ion,  $V_0$  is the microscopic constant.  $\vec{s}_0$  and  $\vec{s}_n$  are the vectors of the magnetic moments of two Fe ions [28]. For the ideal state of the perovskite structure, the Fe–O–Fe bond angle is equal to 180°, so the  $\left[ \vec{r}_{n-0} \times \vec{r}_{n-n} \right]$  factor is zero [29] and the antisymmetric exchange energy term HDM is zero. However, if the Fe–O–Fe bond angle starts to deviate from the ideal state of 180°, HDM will increase. Therefore, the Fe–O–Fe bond angle and Fe–O bond length of the BGSFMC/CN<sub>x</sub>FO composite film are changed with the doping of Ni<sup>2+</sup> (as shown in Table 1), which leads to an increase in HDM and in turn increases magnetization and enhances the magnetic properties. After the Ni<sup>2+</sup>-doped CN<sub>x</sub>FO magnetic bottom layer is combined with the upper BGSFMC, stress is generated at the film interface, which causes the grain growth of the upper BGSFMC. The change in grain size releases more magnetic moments, causing the composite film to increase magnetically. The increase of Fe<sup>3+</sup> and the coexistence of Mn and Co ions make the super exchange of Fe–O–Fe stronger [30]. Therefore, after the Ni<sup>2+</sup>-doped CN<sub>x</sub>FO magnetic bottom layer is combined with the upper BGSFMC, stress occurs at the film interface, which increases the grain size and porosity of the BGSFMC layer. This provides a space

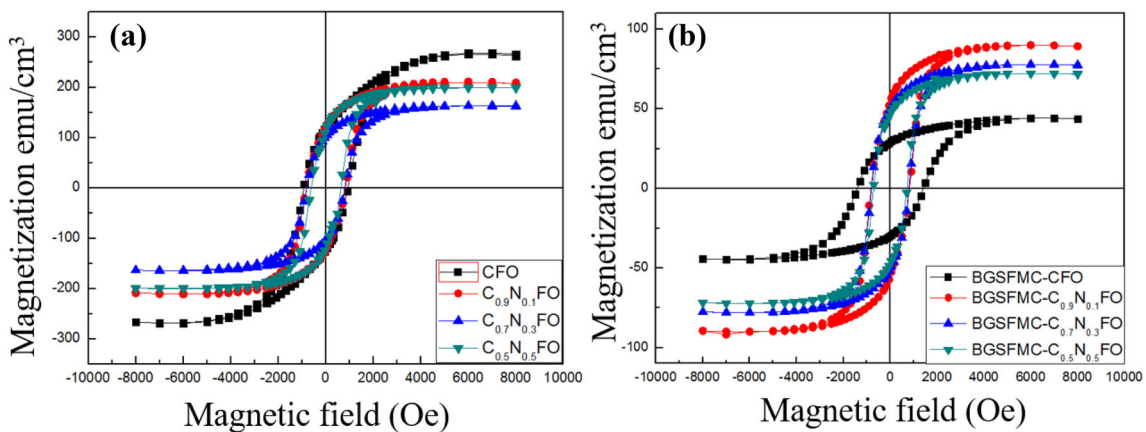


Fig. 4 The hysteresis loop of the CN<sub>x</sub>FO film (a), the hysteresis loop of the BGSFMC/CN<sub>x</sub>FO composite film (b)

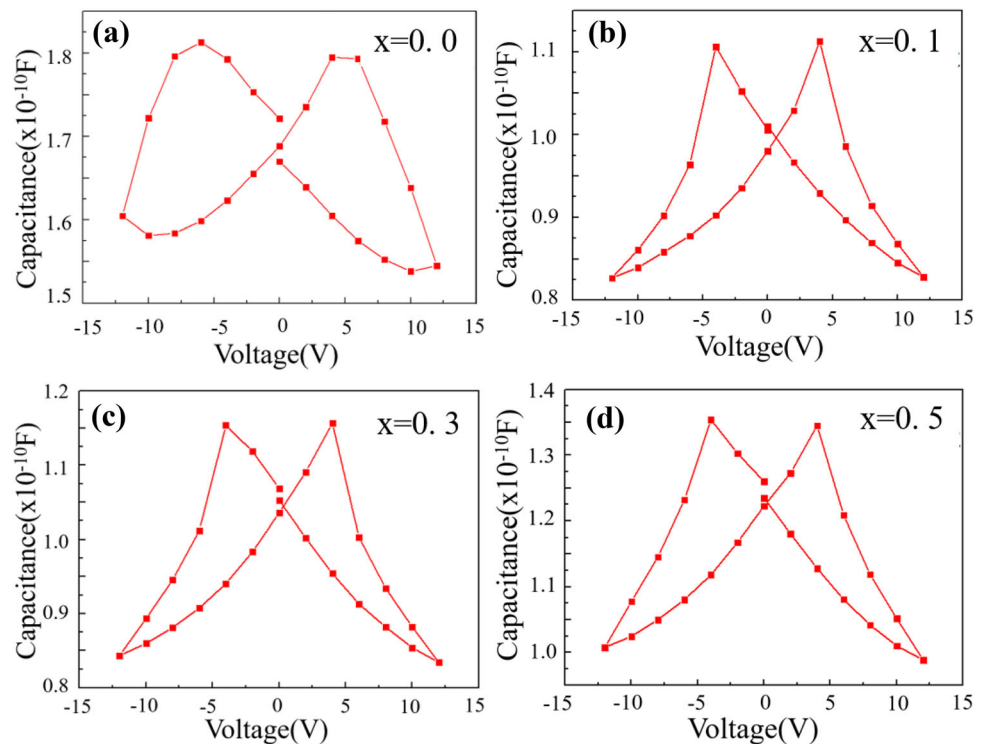
for changes in the Fe–O bond length and Fe–O–Fe bond angle of the BGSFMC layer.

For the BGSFMC/CN<sub>x</sub>FO composite film, a non-linear capacitance–voltage (*C*–*V*) butterfly curve was observed (Fig. 5), which indicates that the films have ferroelectric properties and these *C*–*V* butterfly curves are related to the ferroelectric conversion process [12]. The BGSFMC/CFO film shows a deformed *C*–*V* butterfly curve, which indicates that there is a large obstacle in the domain that inhibits the inversion of the ferroelectric domain. The larger obstacles in the domain are related to the high oxygen vacancy defect concentration and defect complexes in the BGSFMC/CFO composite film (Fig. 5a). A typical symmetrical *C*–*V* butterfly curve is detected in the BGSFMC/CN<sub>0.1</sub>FO composite film, which indicates that the films have good ferroelectric properties [11]. The BGSFMC/CN<sub>0.1</sub>FO composite film has similar capacitance values at voltages of 4 V and –4 V, which are 1.11267E–10 F and 1.10628E–10 F (Fig. 5b), respectively. This indicates that the oxygen vacancy concentration and defect complexes are reduced after Ni<sup>2+</sup> doping, resulting in increased spontaneous polarization. The reduction of intra-domain defects makes the ferroelectric domains easier to flip under the action of an external electric field. These results indicate that the doping of Ni<sup>2+</sup> can

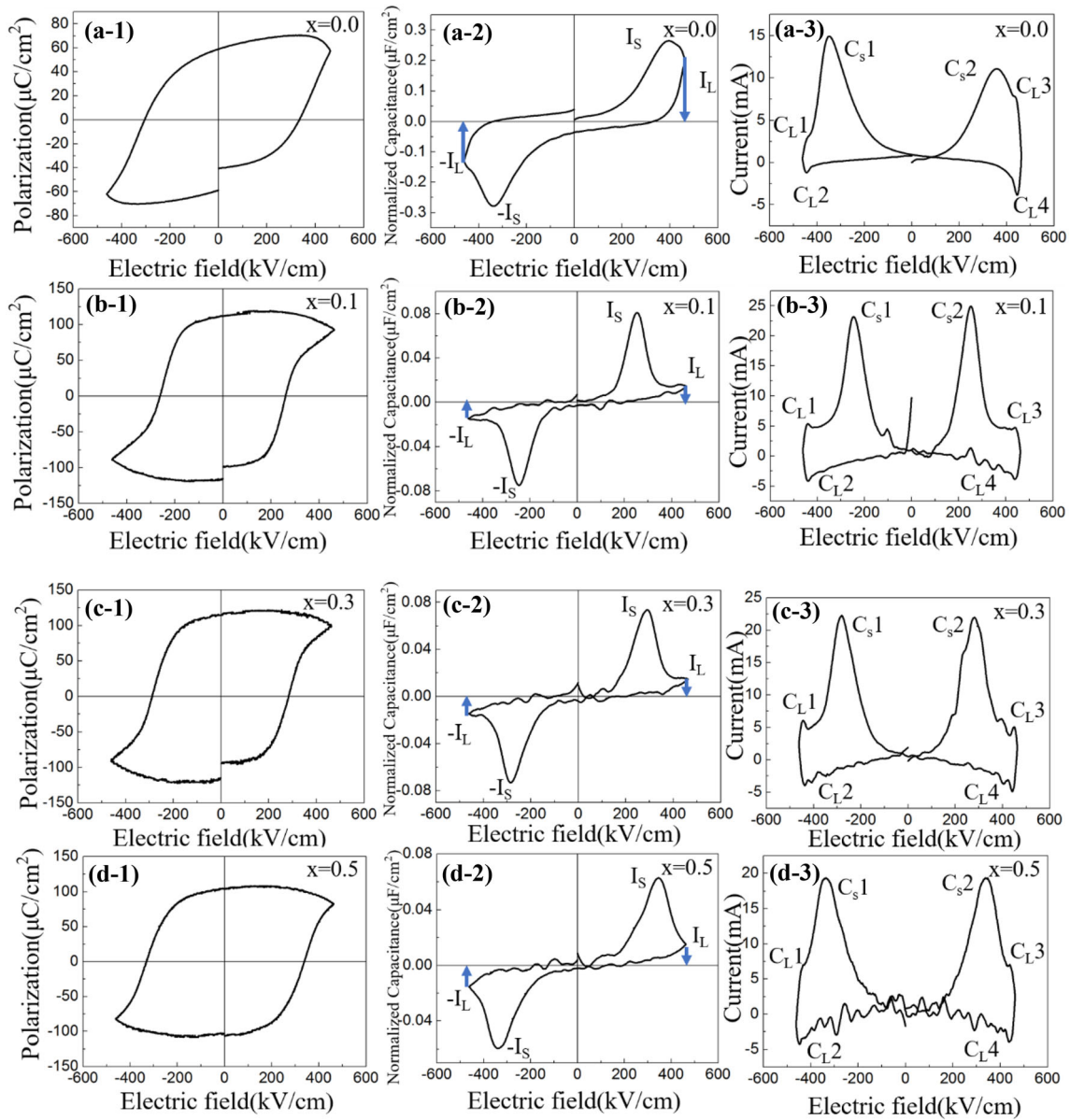
effectively reduce intra-domain defects and enhance the spontaneous polarization.

Figure 6 shows the hysteresis loop, the polarization reversal current curve, and the differential graph of the hysteresis loop of the BGSFMC/CN<sub>x</sub>FO composite film under the test conditions of the test frequency of 1 kHz and 25 V voltage. The electrical hysteresis loop of the BGSFMC/CFO composite film presents a “swelling” state. The polarization reversal current curve shows an obvious “lift” peak. The residual polarization value is 58.97 μC/cm<sup>2</sup>. The polarization leakage current has obvious “towering.” The polarization leakage current (*I*<sub>s</sub>) is 0.26 mA. The polarization reversal current (*I*<sub>s</sub>) is 0.26 mA, the leakage current caused by leakage capacitance (*C*<sub>L</sub>) is 7.83 μC/cm<sup>2</sup>, and the ferroelectric domain switching capacitance peak value (*C*<sub>S</sub>) is 14.91 μF/cm<sup>2</sup> (Fig. 6a). The residual polarization of the BGSFMC/CN<sub>x</sub>FO composite film increases to 104–112 μC/cm<sup>2</sup>. The polarization switching current (*I*<sub>s</sub>) is 0.06–0.08 mA while the *I*<sub>L</sub> is decreased to 0.0144–0.0152 mA. The leakage capacitance (*C*<sub>L</sub>) is reduced to 4.73–6.89 μF/cm<sup>2</sup>. The peak (*C*<sub>S</sub>) of the flip capacitor is enhanced to 19.32–24.9 μF/cm<sup>2</sup> (Fig. 6b–d). The Ni-doped BGSFMC/CN<sub>x</sub>FO composite films have reduced oxygen vacancies and significantly improved ferroelectric domain switching ability and ferroelectric

**Fig. 5** *C*–*V* characteristic curve of the BGSFMC/CN<sub>x</sub>FO composite film







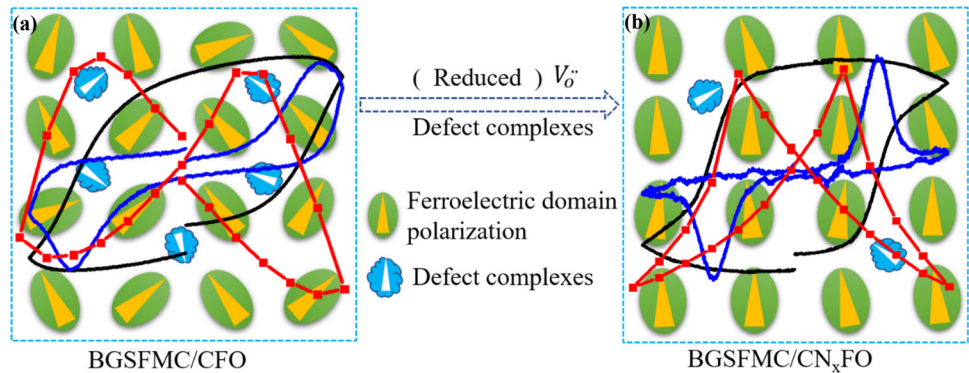
**Fig. 6** Differential diagrams of the electric hysteresis loop, polarization current loop, and electric hysteresis loop of the BGSFMC/CN<sub>x</sub>FO composite film

properties. The intrinsic polarization is enhanced, which is consistent with the results of enhance the spontaneous polarization in Fig. 5b.

Figure 7 is a graph showing the relationship between the ferroelectric domain flipping and the ferroelectric properties of the BGSFMC/CN<sub>x</sub>FO composite films. There are more oxygen vacancies and defect complexes in the BGSFMC/CFO composite film, which will make it difficult for some ferroelectric domains to flip and there is a phenomenon of pseudo polarization. As shown in Fig. 7a, the film shows a deformed hysteresis loop, an

asymmetric C–V curve, and a non-sharp reverse current peak. These confirm that the BGSFMC/CFO composite film has the large leakage conductance and extrinsic polarization, that is, the polarization of BGSFMC/CFO is divided into two parts: iron polarization and leakage conduction polarization. The BGSFMC/CFO composite film has a large number of oxygen vacancies due to its own crystal defects and small grain size, while the oxygen vacancies are mainly concentrated on the grain boundaries. The oxygen vacancies gathering on the grain boundary hinder the transport of electrons on the grain

**Fig. 7** The relationship between the ferroelectric domain switching and the ferroelectric properties of the BGSFMC/ $\text{CN}_x\text{FO}$  composite thin films



boundary. In addition, due to the existence of defect pairs formed by oxygen vacancies and ions, a built-in electric field is formed inside the film. Then with the combined action of the interface energy and in the built-in electric field, the movement and turnover of the ferroelectric domains are suppressed. With the Ni doping, the structure in the BGSFMC/ $\text{CN}_x\text{FO}$  composite film is distorted. The reduction of oxygen vacancies in the film leads to a decrease in defect complexes and an increase in  $\text{Fe}^{3+}$ . The ferroelectric domains of the BGSFMC/ $\text{CN}_x\text{FO}$  composite film are almost completely reversed under the applied voltage. The BGSFMC/ $\text{CN}_{0.1}\text{FO}$  composite film exhibits a large residual polarization value, a compact and symmetrical  $C-V$  curve, and a sharper polarization current reversal peak (Fig. 7b). Therefore, the Ni-doped CFO magnetic underlayer can improve the domain switching ability of the BGSFMC/ $\text{CN}_x\text{FO}$  composite film and enhance the intrinsic ferroelectric properties.

## 4 Conclusion

In this work, the BGSFMC/ $\text{CN}_x\text{FO}$  ( $x = 0.1-0.5$ ) composite film is successfully prepared by the sol-gel method. Ni ions are doped into the  $\text{CN}_x\text{FO}$  magnetic underlayer to form internal stress in the film interface, which induces the structural distortion of the upper BGSFMC. Ni doping causes changes in the Fe–O–Fe bond angle and the Fe–O bond length of the upper BGSFMC, causing spin tilt and releasing magnetism. The interface internal stress can effectively reduce the oxygen vacancy concentration of the upper BGSFMC, which inhibits the conversion from  $\text{Fe}^{3+}$  to  $\text{Fe}^{2+}$  and enhances the Fe–O–Fe super exchange interaction. Compared with the BGSFMC/CFO composite film, the ferromagnetic properties of

the BGSFMC/ $\text{CN}_x\text{FO}$  composite film are significantly enhanced, and the residual magnetization of  $48.29-56.94 \text{ emu/cm}^3$  is obtained. Meanwhile, the doping of Ni ions into the  $\text{CN}_x\text{FO}$  layer inhibits the formation of the defect complexes in the BGSFMC layer. The residual polarization value of the BGSFMC/ $\text{CN}_x\text{FO}$  composite film is increased to  $104-112 \mu\text{C/cm}^2$ . The polarization reversal current ( $I_s$ ) is  $0.06-0.08 \text{ mA}$ . The domain switching ability and the ferroelectric performance are significantly improved and the intrinsic polarization performance is also enhanced. Ni ions are doped into the  $\text{CN}_x\text{FO}$  magnetic underlayer to induce structural changes in the upper BGSFMC, which enhances the ferroelectric properties of the composite film while enhancing the ferromagnetic properties. This provides more choice materials for multifunctional, high-performance storage devices and photoelectric sensors.

## Acknowledgements

This work is supported by the Shaanxi Province Key Research and Development Plan (2018GY-107), the Project of the National Natural Science Foundation of China (51372145), Natural Science Basic Research Plan in Shaanxi Province of China (2020JQ-730), and the Graduate Innovation Fund of Shaanxi University of Science & Technology (SUST-A04).

**Supplementary Information:** The online version contains supplementary material available at <http://doi.org/10.1007/s10854-020-05203-8>.

## References

1. Y. Tokura, S. Seki, N. Nagaosa, Multiferroics of spin origin. *Rep. Prog. Phys.* **77**, 076501 (2014)
2. J. Ma, J. Hu, Z. Li, C.W. Nan, Recent progress in multiferroic magnetoelectric composites: from bulk to thin films. *Adv. Mater.* **23**, 1062–1087 (2011)
3. K. Chakrabarti, K. Das, B. Sarkar, S. Ghosh, S.K. De, G. Sinha, J. Lahtinen, Enhanced magnetic and dielectric properties of Eu and Co co-doped BiFeO<sub>3</sub> nanoparticles. *Appl. Phys. Lett.* **101**, 1–6 (2012)
4. D. Lin, Q. Zheng, Y. Li, Y. Wan, Q. Li, W. Zhou, Microstructure, ferroelectric and piezoelectric properties of Bi<sub>0.5</sub>K<sub>0.5</sub>TiO<sub>3</sub>-modified BiFeO<sub>3</sub>-BaTiO<sub>3</sub> lead-free ceramics with high Curie temperature. *J. Eur. Ceram. Soc.* **33**, 3023–3036 (2013)
5. J. Seidel, L.W. Martin, Q. He, Q. Zhan, Y.H. Chu, A. Rother, M.E. Hawkrige, P. Maksymovych, P. Yu, M. Gajek, N. Balke, S.V. Kalinin, S. Gemming, F. Wang, G. Catalan, J.F. Scott, N.A. Spaldin, J. Orenstein, R. Ramesh, Conduction at domain walls in oxide multiferroics. *Nat. Mater.* **8**, 229–234 (2009)
6. F. Zavaliche, S.Y. Yang, T. Zhao, Y.H. Chu, M.P. Cruz, C.B. Eom, R. Ramesh, Multiferroic BiFeO<sub>3</sub> films: domain structure and polarization dynamics. *Phase Transit.* **79**, 991–1017 (2006)
7. I. Sosnowska, T.P. Neumaier, E. Steichele, Spiral magnetic ordering in bismuth ferrite. *J. Phys. C Solid State Phys.* **15**, 4835–4846 (1982)
8. Y. Ahn, J.Y. Son, Multiferroic properties and ferroelectric domain structures of Yb-doped BiFeO<sub>3</sub> thin films on glass substrates. *Physica B Condens. Matter.* **558**, 24–27 (2019)
9. K.S. Kumar, S. Ramu, A. Sudharani, M. Ramanadha, G. Murali, R.P. Vijayalakshmi, Enhanced magnetic and dielectric properties of Gd doped BiFeO<sub>3</sub>: Er nanoparticles synthesized by sol–gel technique. *Physica E Low Dimens. Syst. Nanos-struct.* **115**, 113689 (2020)
10. W. Mao, Q. Yao, Y. Fan, Y. Wang, X. Wang, Y. Pu, X. Li, Combined experimental and theoretical investigation on modulation of multiferroic properties in BiFeO<sub>3</sub> ceramics induced by Dy and transition metals co-doping. *J. Alloys Compd.* **784**, 117–124 (2019)
11. Y. Liu, G. Tan, M. Guo, Z. Chai, L. Lv, M. Xue, X. Ren, J. Li, H. Ren, A. Xia, Multiferroic properties of La/Er/Mn/Co multi-doped BiFeO<sub>3</sub> thin films. *Ceram. Int.* **45**, 11765–11775 (2019)
12. Z. Chai, G. Tan, Z. Yue, W. Yang, M. Guo, H. Ren, A. Xia, M. Xue, Y. Liu, L. Lv, Y. Liu, Ferroelectric properties of BiFeO<sub>3</sub> thin films by Sr/Gd/Mn/Co multi-doping. *J. Alloys Compd.* **746**, 677–687 (2018)
13. N. Hamdaoui, Y. Azizian-Kalendaragh, M. Khelifi, L. Beji, Structural, magnetic and dielectric properties of Ni<sub>0.6</sub>Mg<sub>0.4</sub>Fe<sub>2</sub>O<sub>4</sub> ferromagnetic ferrite prepared by sol gel method. *Ceram. Int.* **45**, 16458–16465 (2019)
14. S. Yonatan Mulushoa, N. Murali, M. Tulu Wegayehu, V. Veeraiah, K. Samatha, Investigation of structural, DC-resistivity and magnetic properties of Mg ferrite. *Mater. Today Proc.* **5**, 26460–26468 (2018)
15. H.L. Mo, D.M. Jiang, C.M. Wang, W.G. Zhang, J. Sen Jiang, Magnetic, dielectric and magnetoelectric properties of CoFe<sub>2</sub>O<sub>4</sub>-Bi<sub>0.85</sub>La<sub>0.15</sub>FeO<sub>3</sub> multiferroic composites. *J. Alloys Compd.* **579**, 187–191 (2013)
16. M. Guo, G. Tan, Y. Zheng, W. Liu, H. Ren, A. Xia, Interfacial characteristics and multiferroic properties of ion-doped BiFeO<sub>3</sub>/NiFe<sub>2</sub>O<sub>4</sub> thin films. *J. Appl. Phys.* **121**, 104409–1831 (2017)
17. G. Tan, Z. Chai, Y. Zheng, Z. Yue, W. Yang, M. Guo, H. Ren, A. Xia, L. Lv, Y. Liu, Tunable structural transition and multiferroic properties of the composite thin films through the structural transition of magnetic layer. *J. Eur. Ceram. Soc.* **38**, 4463–4475 (2018)
18. Z. Chai, G. Tan, Z. Yue, M. Xue, Y. Liu, L. Lv, H. Ren, A. Xia, Structural transition, defect complexes and improved ferroelectric behaviors of Bi<sub>0.88</sub>Sr<sub>0.03</sub>Gd<sub>0.09</sub>Fe<sub>0.94</sub>Mn<sub>0.04</sub>Co<sub>0.02</sub>O<sub>3</sub>/Co<sub>1-x</sub>Mn<sub>x</sub>Fe<sub>2</sub>O<sub>4</sub> bilayer thin films. *Ceram. Int.* **44**, 15770–15777 (2018)
19. K. Omri, I. Najeh, L. El Mir, Influence of annealing temperature on the microstructure and dielectric properties of ZnO nanoparticles. *Ceram. Int.* **42**, 8940 (2016)
20. K. Omri, A. Bettaibi, K. Khirouni, L. El Mir, The optoelectronic properties and role of Cu concentration on the structural and electrical properties of Cu doped ZnO nanoparticles. *Physica B Condens. Matter* **537**, 167 (2018)
21. K. Omri, A. Alyamani, L. El Mir, Surface morphology, microstructure and electrical properties of Ca-doped ZnO thin films. *J. Mater. Sci. Mater. Electron.* **30**, 16606 (2019)
22. D. Kothari, V. Raghavendra Reddy, V.G. Sathe, A. Gupta, A. Banerjee, A.M. Awasthi, Raman scattering study of polycrystalline magnetoelectric BiFeO<sub>3</sub>. *J. Magn. Magn. Mater.* **320**, 548–552 (2008)
23. R.S. Yadav, J. Havlica, M. Hnatko, P. Šajgalík, C. Alexander, M. Palou, E. Bartoničková, M. Boháč, F. Frajkorová, J. Masilko, M. Zmrzlý, L. Kalina, M. Hajdúchová, V. Enev, Magnetic properties of Co<sub>1-x</sub>Zn<sub>x</sub>Fe<sub>2</sub>O<sub>4</sub> spinel ferrite nanoparticles synthesized by starch-assisted sol–gel auto-combustion method and its ball milling. *J. Magn. Magn. Mater.* **378**, 190–199 (2015)
24. G.L. Yuan, S.W. Or, H.L.W. Chan, Raman scattering spectra and ferroelectric properties of Bi<sub>1-x</sub>Nd<sub>x</sub>FeO<sub>3</sub> (x = 0–0.2) multiferroic ceramics. *J. Appl. Phys.* **101**, 0–5 (2007)

25. Y. Zheng, G. Tan, A. Xia, H. Ren, Structure and multiferroic properties of multi-doped  $\text{Bi}_{1-x}\text{Er}_x\text{Fe}_{0.96}\text{Mn}_{0.02}\text{Co}_{0.02}\text{O}_3$  thin films. *J. Alloys Compd.* **684**, 438–444 (2016)
26. F. Aziz, P. Pandey, M. Chandra, A. Khare, D.S. Rana, K.R. Mavani, Surface morphology, ferromagnetic domains and magnetic anisotropy in  $\text{BaFeO}_{3-\delta}$  thin films: correlated structure and magnetism. *J. Magn. Mater.* **356**, 98–102 (2014)
27. M.M. Shirolkar, C. Hao, X. Dong, T. Guo, L. Zhang, M. Li, H. Wang, Tunable multiferroic and bistable/complementary resistive switching properties of dilutely Li-doped  $\text{BiFeO}_3$  nanoparticles: an effect of aliovalent substitution. *Nanoscale* **6**, 4735–4744 (2014)
28. B. Ahmmad, M.Z. Islam, A. Billah, M.A. Basith, Anomalous coercivity enhancement with temperature and tunable exchange bias in Gd and Ti co-doped  $\text{BiFeO}_3$  multiferroics. *J. Phys. D Appl. Phys.* **49**, 95001 (2016)
29. C. Ederer, C.J. Fennie, Electric-field switchable magnetization via the Dzyaloshinskii–Moriya interaction:  $\text{FeTiO}_3$  versus  $\text{BiFeO}_3$ . *J. Phys. Condens. Matter.* **20**, 434219 (2008)
30. Y. Zhang, Y. Wang, J. Qi, Y. Tian, M. Sun, J. Zhang, T. Hu, M. Wei, Y. Liu, J. Yang, Enhanced magnetic properties of  $\text{BiFeO}_3$  thin films by doping: analysis of structure and morphology. *Nanomaterials* **8**, 1–13 (2018)

**Publisher's Note** Springer Nature remains neutral with regard to jurisdictional claims in published maps and institutional affiliations.